COMPARISON OF TWO-DIMENSIONAL AND THREE-DIMENSIONAL MAPPING OF IONOSPHERIC ELECTRIC FIELD

C. G. Park

Radioscience Laboratory, Stanford University, Stanford, California 94305

Abstract. Numerical techniques are used to compare two-dimensional and three-dimensional analyses of the spreading of ionospheric electric fields. Specific cases are considered in which a source electric field is applied at 150-km altitude and within a limited horizontal distance L. It is found that horizontal spreading of fields at ionospheric heights can be accurately calculated by using a two-dimensional model with height-integrated conductivities, provided that L is 10 km or greater. For L < 10 km a full three-dimensional model must be used. Three-dimensional calculations must also be used to relate electric fields measured at balloon altitudes (~30 km) to overhead ionospheric fields if L < 100 km. Calculated ionospheric fields depend strongly on horizontal conductivity gradients, fields spreading more easily in the direction of decreasing conductivity.

Introduction

In many problems involving calculations of electric fields and currents in the ionosphere it is general practice to treat the ionosphere like a thin sheet whose electrical properties are described by effective height-integrated conductivities [Baker and Martyn, 1953; Fejer, 1953; Vasyliunas, 1970; Boström, 1974; Wolf, 1975; Nisbet et al., 1978]. This approach is very useful, particularly when numerical solutions must be used, since many unwieldy three-dimensional problems can be reduced to two-dimensional problems of manageable size. However, it is important to know when such a simplified approach is valid and when full three-dimensional solutions must be sought.

The concept of height-integrated conductivity was first introduced in atmospheric dynamo theories in which currents were assumed to be confined within the ionosphere [Baker and Martyn, 1953; Fejer, 1953]. Later, Swift [1972] showed that this approach is valid even when currents flow between the ionosphere and the magnetosphere. In his analysis, Swift assumed an electric field, harmonically varying in the horizontal direction, at the top of the ionosphere and then calculated resulting electric field and current distributions below. He found that height-integrated currents evaluated this way were in good agreement with the values obtained from simpler two-dimensional analysis using height-integrated conductivities, provided that the spatial wavelength of the assumed electric field was of the order of 10 km or greater.

In this study we consider how an electric field applied in a limited region of the ionosphere spreads out horizontally as well as downward into the lower atmosphere. Figure 1 illustrates the geometry of the problem. A Cartesian coordinate system is used with the z axis pointing vertically upward. We assume a constant applied electric field E_{yo} at z = 150 km, limited in horizontal extent to $x \leq 0$ and $-(L/z) \leq y \leq (L/z)$. We use a three-dimensional numerical analysis to calculate how this applied electric field spreads to the region $x > 0$ and $z \leq 150$ km. The ionospheric electric field calculated this way for $x > 0$ is compared with the results of equivalent two-dimensional analysis using height-integrated conductivities. It is found that at ionospheric heights, two- and three-dimensional results are identical for $L \geq 10$ km, in agreement with earlier results by Swift [1972]. We also calculate electric field variations as a function of x that would be measured by a balloon-borne probe at 30-km altitude [e.g., Mozer and Serlin, 1969]. The effects of horizontal conductivity gradients in both two- and three-dimensional analyses are also examined.

Formulation of the Problem

The basic equations to be solved are

$$\nabla \cdot \vec{J} = 0 \tag{1}$$

$$\vec{J} = \overleftrightarrow{\sigma}\vec{E} \tag{2}$$

$$\vec{E} = -\nabla \Phi \tag{3}$$

where $\vec{J}$ is the electric current density, $\vec{E}$ is the electric field, $\overleftrightarrow{\sigma}$ is the conductivity tensor, and Φ is the electric potential. If we adopt a Cartesian coordinate system with the z axis pointing upward and assume a geomagnetic field directed vertically downward, (2) can be written as

$$J_x = \sigma_p E_x + \sigma_H E_y \tag{4}$$

$$J_y = \sigma_p E_y - \sigma_H E_x \tag{5}$$

$$J_z = \sigma_o E_z \tag{6}$$

where σ_o, σ_p, and σ_H are the specific, Pedersen, and Hall conductivities, respectively. Equations (1) and (3)-(6) can be combined to yield

$$\sigma_p \frac{\partial^2\Phi}{\partial x^2} + \sigma_p \frac{\partial^2\Phi}{\partial y^2} + \left(\frac{\partial\sigma_p}{\partial x} - \frac{\partial\sigma_H}{\partial y}\right)\frac{\partial\Phi}{\partial x} + \left(\frac{\partial\sigma_H}{\partial x} + \frac{\partial\sigma_p}{\partial y}\right)\frac{\partial\Phi}{\partial y} + \frac{\partial\sigma_o}{\partial z}\frac{\partial\Phi}{\partial z} = 0 \tag{7}$$

This equation is subject to boundary conditions at z = 0 and 150 km and at $x = y = \pm\infty$. We set $\Phi = 0$ at z = 0. At z = 150 km we specify Φ as a function of x and y for $x \leq 0$ and set $\partial\Phi/\partial z = 0$ for $x > 0$. At $x = y = \pm\infty$ we assume that current flows in the vertical direction only. With this assumption the other necessary boundary condi-

Paper number 8A1364.
0148-0227/79/008A-1364$01.00

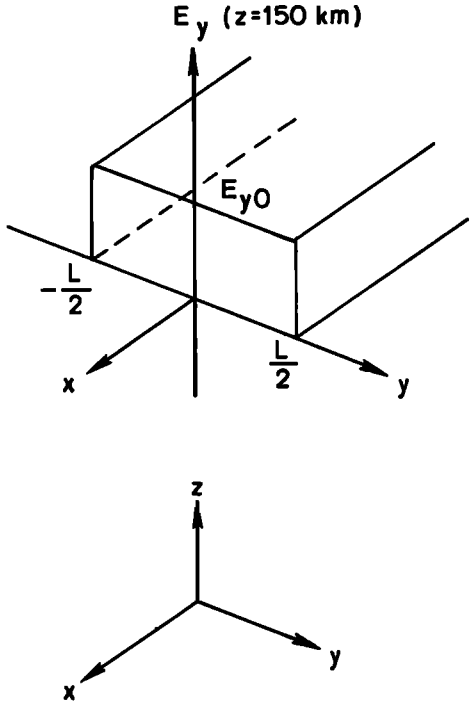

Fig. 1. The coordinate system and the geometry of the problem.

tions at $x = y = \pm\infty$ can be easily calculated from

$$\Phi(\pm\infty, \pm\infty, z) = \left(\int_0^z \frac{dz}{\sigma_o} \Big/ \int_0^{150\text{ km}} \frac{dz}{\sigma_o}\right) \Phi(\pm\infty, \pm\infty, 150\text{ km})$$

In order to facilitate numerical solutions of (7) we introduce new variables $p = \arctan(\alpha x)$ and $q = \arctan(\beta y)$, so that they range from $-(\pi/2)$ to $+(\pi/2)$ as x and y vary from $-\infty$ to $+\infty$. Equation (7) then becomes

$$s^2\sigma_p \frac{\partial^2\Phi}{\partial p^2} + t^2\sigma_p \frac{\partial^2\Phi}{\partial q^2} + \sigma_o \frac{\partial^2\Phi}{\partial z^2} + \left(s \frac{\partial\sigma_p}{\partial x} - s \frac{\partial\sigma_H}{\partial y} - 2s^2\alpha x\sigma_p\right)\frac{\partial\Phi}{\partial p} + \left(t \frac{\partial\sigma_H}{\partial x} + t \frac{\partial\sigma_p}{\partial y} - 2t^2\beta y\sigma_p\right)\frac{\partial\Phi}{\partial q} + \frac{\partial\sigma_o}{\partial z}\frac{\partial\Phi}{\partial z} = 0 \quad (8)$$

$$s = \frac{\alpha}{1 + \alpha^2x^2} \quad (9)$$

$$t = \frac{\beta}{1 + \beta^2y^2} \quad (10)$$

If we assume that E_x and E_y are independent of z, (4) and (5) can be integrated over z to yield two-dimensional equations

$$I_x = \Sigma_p E_x + \Sigma_H E_y \quad (11)$$

$$I_y = \Sigma_p E_y - \Sigma_H E_y \quad (12)$$

where

$$I = \int_0^\infty J\, dz$$

and

$$\Sigma = \int_0^\infty \sigma\, dz$$

Combining (11) and (12) with (1) and (3), we obtain

$$\Sigma_p \frac{\partial^2\Phi}{\partial x^2} + \Sigma_p \frac{\partial^2\Phi}{\partial y^2} + \left(\frac{\partial\Sigma_p}{\partial x} - \frac{\partial\Sigma_H}{\partial y}\right)\frac{\partial\Phi}{\partial x} + \left(\frac{\partial\Sigma_p}{\partial y} + \frac{\partial\Sigma_H}{\partial x}\right)\frac{\partial\Phi}{\partial y} = 0 \quad (13)$$

Boundary conditions are specified in terms of Φ at $x = 0$, $x = +\infty$, and $y = \pm\infty$. Again, we introduce new variables $p = \arctan(\alpha x)$ and $q = \arctan(\beta y)$, as we did in the three-dimensional case. Equation (13) then becomes

$$s^2\Sigma_p \frac{\partial^2\Phi}{\partial p^2} + t^2\Sigma_p \frac{\partial^2\Phi}{\partial q^2} + \left(s \frac{\partial\Sigma_p}{\partial x} - s \frac{\partial\Sigma_H}{\partial y} - 2s^2\alpha x\Sigma_p\right)\frac{\partial\Phi}{\partial p} + \left(t \frac{\partial\Sigma_p}{\partial y} + t \frac{\partial\Sigma_H}{\partial x} - 2t^2\beta y\Sigma_p\right)\frac{\partial\Phi}{\partial q} = 0 \quad (14)$$

where s and t are as defined previously by (9) and (10).

In the next section we examine the conditions under which we may assume E_x and E_y to be independent of z and use (14) instead of (8).

Calculations and Results

In this section we describe numerical solutions of (8) and (14) for the class of problems depicted in Figure 1. The general procedure that we adopted was to set up two-dimensional (p, q) or three-dimensional (p, q, z) grids, assume an initial value of Φ at each grid point, and keep integrating through a line iteration scheme [e.g., Diaz et al., 1958] until a specified accuracy was achieved. Once Φ is known, $\vec{E}$ is easily obtained

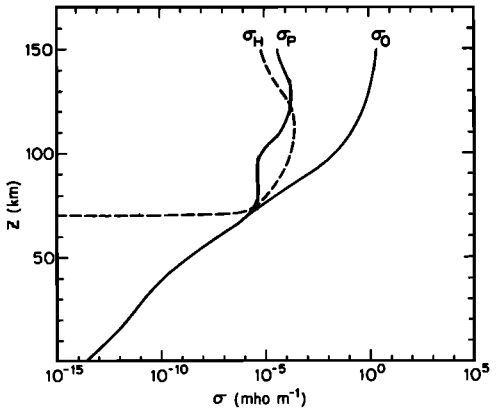

Fig. 2. Height variations of specific (σ_0), Pedersen (σ_P), and Hall (σ_H) conductivities.

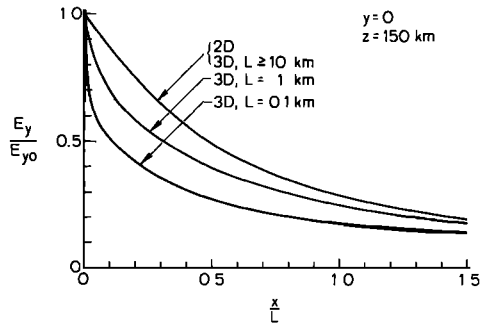

Fig. 3. Calculated ionospheric electric field as a function of horizontal distance from the source based on two-dimensional and three-dimensional models. Both E_y and x are normalized.

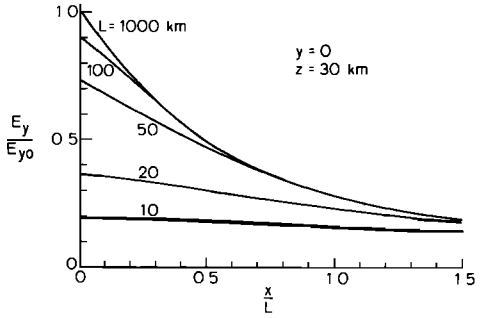

Fig. 5. Three-dimensional results of E_y at 30-km altitude for different values of L.

from (3). Grid spacings of 0.05 in p and q coordinates and 3 km in the z coordinate were found to be a reasonable compromise between accuracy and economy. The values of α and β were adjusted depending on the scale size L of the imposed electric field so as to provide adequate grid density in the region of interest. The amount of computing and storage required is considerable in the three-dimensional case. The computations reported here were done on the Cray 1 computer at the National Center for Atmospheric Research.

Figure 2 shows vertical profiles of σ_o, σ_p, and σ_H that will serve as the 'base' profiles in all of our calculations [Park and Dejnakarintra, 1977a, b]. The corresponding height-integrated conductivities are Σ_p = 5.6 mho and Σ_H = 8.5 mho. When we consider the effects of horizontal conductivity gradients, these base profiles will be multiplied by appropriate spatial functions. We will first discuss electric field spreading in the absence of horizontal conductivity gradients.

Horizontal spreading in the ionosphere. Given a constant electric field E_{yo} at z = 150 km, $x \leq 0$, and $-(L/2) \leq y \leq (L/2)$, we want to examine how this field spreads horizontally to the region x > 0. Before looking at the numerical results we can anticipate the general behavior of the solutions by referring to (13). If we let all gradients of Σ_p and Σ_H equal zero, (13) reduces to a Laplace equation:

$$\frac{\partial^2 \Phi}{\partial x^2} + \frac{\partial^2 \Phi}{\partial y^2} = 0 \qquad (15)$$

Solutions to this equation are obviously independent of L as well as of Σ_p and Σ_H. As was stated previously, the three-dimensional problem reduces to (13), and therefore to (15), if we assume that E_x and E_y are independent of z. This assumption is valid for large L; our aim is to find out at what point this assumption breaks down and three-dimensional equations must be employed.

Figure 3 shows the two- and three-dimensional results in normalized form. The ordinate is the normalized E_y at y = 0 and z = 150 km, and the abscissa is the x coordinate in units of L. The top curve shows the two-dimensional solution, which is indistinguishable from the three-dimensional solutions for $L \geq 10$ km. The two lower curves show three-dimensional solutions for L = 1 and 0.1 km, respectively. It is clear that two-dimensional approximation is valid for scale sizes down to 10 km. This is in agreement with earlier results by Swift [1972].

Downward spreading of ionospheric E fields. We have just discussed how E fields spread horizontally at 150-km altitude. Now we consider how these fields spread to lower altitudes by using the three-dimensional model. The physical situation is identical to that considered above. Figure 4 shows how E_y diminishes with decreasing altitude for the L = 10 km case. E_y maps down to 80-km altitude with very little attenuation, because large ratios of σ_o to σ_p tend to make magnetic field lines look like equipotentials. Below 80 km, E_y is attenuated rapidly for small values of x, so that at z = 30 km, E_y is only a weak function of x. This is simply due to the fact that large wavelength components of the source spectrum (Fourier spectrum of the applied square

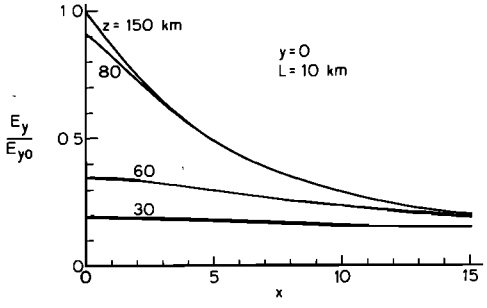

Fig. 4. Normalized E_y as a function of x at different altitudes for L = 10 km. A three-dimensional model was used in the calculations.

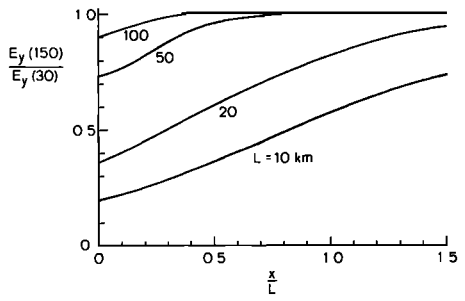

Fig. 6. The mapping factor for E_y from 150-km altitude for different values of L.

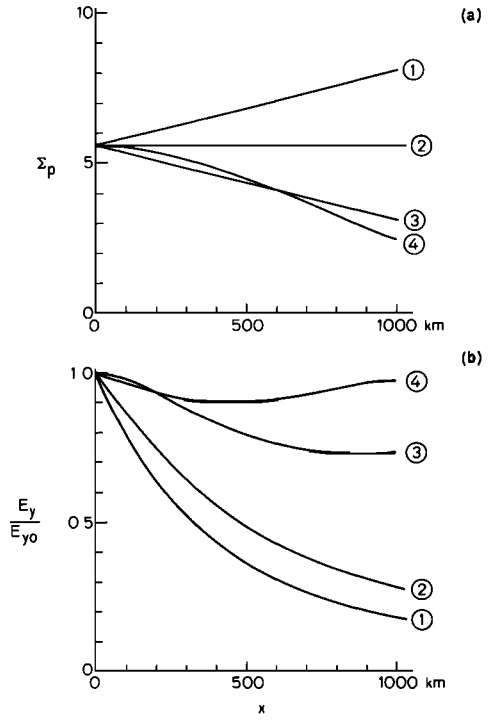

Fig. 7. (a) Assumed variations of height-integrated Pedersen conductivity with horizontal distance x. (b) Calculated E_y as a function of x for different horizontal conductivity variations.

wave form) that spread out farther in x also map down more efficiently to lower altitudes.

Figure 5 shows, in the same format as in Figure 3, E field variations at y = 0 and z = 30 km. The L = 1000 km curve is identical to the top curve in Figure 3, since E field variations at z = 150 km map down to z = 30 km with practically no attenuation. This is in agreement with previous results [Kellogg and Weed, 1969; Mozer and Serlin, 1969; Boström and Fahleson, 1977; Park, 1976; Chiu, 1974]. We note that attenuation generally increases as L decreases. Furthermore, E becomes nearly independent of x as L is reduced to ~10 km. If horizontal electric fields were measured by a probe mounted on a balloon at 30-km altitude, we may ask how accurately such measurements represent overhead ionospheric fields at, say, 150-km altitude. The answer to this question is provided in Figure 6, where the 'mapping factor,' or the ratio of E_y at 150 km to E_y at 30 km, is plotted as a function of x/L for different values of L. For small values of L the mapping factor increases toward unity with increasing x/L. This means that the electric field measured on a balloon becomes a better approximation of the overhead ionospheric field as the balloon moves farther away from the source. In any case, the field strength measured on a balloon is always less than the overhead ionospheric field strength, even when the ionospheric field has strong horizontal gradients.

Effects of horizontal conductivity gradients. First, we consider a two-dimensional problem where $\partial\Sigma/\partial y = 0$ but $\partial\Sigma/\partial x \neq 0$. Equation (14) is solved as before, with Σ_p and Σ_H modified by a common multiplication factor g(x). Figure 7a shows variations of Σ_p for four different cases considered. In cases 1 and 3, g(x) varies linearly with x. (In actual computations, linear variations continued up to x = 2000 km, beyond which g became constant with x.) In case 4, g(x) is a Gaussian function. Case 2 with no conductivity gradient will serve as reference. Figure 7b shows corresponding E field results for L = 1000 km. It is clear that electric field penetrates more easily in the direction of decreasing conductivity and that the degree of penetration depends strongly on conductivity gradients, particularly if the gradient is negative.

The magnitude of the conductivity gradient effect depends on the scale size of the electric field under consideration. For a given conductivity gradient, its effect diminishes as the scale size L decreases. Although it is not obvious from (14), it turns out that if the gradients are specified in terms of L, the same gradient $\partial\Sigma/\partial(x/L)$ gives the same electric field distribution E(x/L). Thus the curves in Figure 7 would be valid for all values of L if the horizontal axes were normalized by dividing them by 1000 km.

In the three-dimensional case, horizontal conductivity gradients may depend on the altitude. We saw earlier that horizontal spreading of ionospheric electric field can be accurately calculated by an equivalent two-dimensional model as long as $L \geq 10$ km. This is still true in the presence of horizontal conductivity gradients. Therefore for $L \geq 10$ km, electric field distribution at ionospheric heights will be affected only by gradients in height-integrated conductivities; detailed height variations of σ and $\partial\sigma/\partial x$ are not important. For $L < 10$ km, one must, of course, solve the full three-dimensional problem.

Conclusions

The following conclusions can be drawn from the results described above. (1) Horizontal spreading of ionospheric electric fields (above ~80-km altitude) can be accurately calculated by using a two-dimensional model with height-integrated conductivities, provided that the scale size of the imposed field L is 10 km or greater. This is true independent of horizontal conductivity gradients. (2) Three-dimensional calculations must be used to relate ionospheric fields measured at 30 km to overhead ionospheric fields if $L < 100$ km. (3) In the presence of horizontal conductivity gradients, electric field spreads more easily in the direction of decreasing conductivity. For given conductivity gradients, their effect diminishes with decreasing L. However, if a normalized coordinate w = x/L is used, the effect of $\partial\sigma/\partial w$ on E(w) is the same, independent of L.

Acknowledgements. This work was supported by the Atmospheric Sciences Section of the National Science Foundation under grant ATM74-20084. Computer calculations were done at the National Center for Atmospheric Reearch, which is funded by the National Science Foundation.

The Editor thanks F. S. Mozer for his assistance in evaluating this brief report.

References

Baker, W. G., and D. F. Martyn, Electric currents in the ionosphere, 1, The conductivity, Phil. Trans. Roy. Soc. London, Ser. A., 246, 281, 1953.

Boström, R., Ionosphere-magnetosphere coupling, in Magnetospheric Physics, edited by B. M. McCormac, p. 45, D. Reidel, Hingham, Mass., 1974.

Boström, R., and U. Fahleson, Vertical propagation of time-dependent electric fields in the atmosphere and ionosphere, in Electrical Processes in Atmospheres, edited by H. Dolezalek and R. Reiter, p. 529, Darmstadt, Germany, D. Steinkopff Verlag, 1977.

Chiu, Y. T., Self-consistent electrostatic field mapping in the high-latitude ionosphere, J. Geophys. Res., 79, 2790, 1974.

Díaz, J. B., R. F. Chippinger, G. Friedman, E. Isaacson, and R. Richtmeyer, Particle differential equations, in Handbook of Automation, Computation and Control, vol. 1, edited by E. M. Grabbe, S. Ramo, and D. E. Wooldridge, p. 14, John Wiley, New York, 1958.

Fejer, J. A., Semidiurnal currents and electron drifts in the ionosphere, J. Atmos. Terr. Phys., 4, 184, 1953.

Kellogg, P. J., and M. Weed, Balloon measurements of ionospheric electric fields, in Planetary Electrodynamics, vol. 2, edited by S. C. Coroniti and J. Hughes, p. 431, Gordon and Breach, New York, 1969.

Mozer, F. S., and R. Serlin, Magnetospheric electric field measurements with balloons, J. Geophys. Res., 74, 4739, 1969.

Nisbet, J. S., M. J. Miller, and L. A. Carpenter, Currents and electric fields in the ionosphere due to field-aligned auroral currents, J. Geophys. Res., 83, 2647, 1978.

Park, C. G., Downward mapping of high-latitude ionospheric field to the ground, J. Geophys. Res., 81, 168, 1976.

Park, C. G., and M. Dejnakarintra, The effects of magnetospheric convection on atmospheric electric fields in the polar cap, in Electrical Processes in Atmospheres, edited by H. Dolezalek and R. Reiter, P. 536, D. Steinkopff Verlag, Darmstadt, Germany, 1977a.

Park, C. G., and M. Dejnakarintra, Thundercloud electric fields in the ionosphere, in Electrical Processes in Atmospheres, edited by H. Dolezalek and R. Reiter, p. 544, D. Steinkopff Verlag, Darmstadt, Germany, 1977b.

Swift, D. W., Effective height-integrated conductivity of the ionosphere, J. Geophys. Res., 77, 1279, 1972.

Vasyliunas, V. M., Mathematical models of magnetospheric convection and its coupling to the ionosphere, in Particles and Fields in the Magnetosphere, edited by B. M. McCormac, D. Reidel, Hingham, Mass., 1970.

Wolf, R. A., Ionosphere-magnetosphere coupling, Space Sci. Rev., 17, 537, 1975.

(Received August 9, 1978;
revised December 5, 1978;
accepted December 11, 197.)